

Sensitivity analysis on chaotic dynamical system by Non-Intrusive Least Square Shadowing (NILSS)

Angxiu Ni^{a,*}, Qiqi Wang^a

^a*Aeronautics and Astronautics, MIT, 77 Mass Ave, Cambridge, MA 02139, USA*

Abstract

This paper develops the tangent Non-Intrusive Least Square Shadowing (NILSS) method, which computes the sensitivity for long time averaged objective in chaotic dynamical systems. In NILSS, a tangent solution is represented as a linear combination of a inhomogeneous tangent solution and some homogeneous tangent solutions. Then we solve a least square problem under this new representation. As a result, NILSS is easier to implement with existing solvers. For chaotic systems with large degrees of freedom but low dimensional attractors, NILSS has low computational cost. NILSS is applied to two chaotic PDE systems: the Lorenz 63 system, and a CFD simulation of a backward-facing step. In both cases, the sensitivities computed by NILSS can reflect the trend in the objectives.

Keywords: Sensitivity analysis, linear response, tangent equation, chaos, dynamical systems, uniform hyperbolicity, ergodicity, least square shadowing

1. Introduction

Many important phenomena in engineering are chaotic, such as problems involving turbulent flows[1] or fluid-structure interactions[2]. For these chaotic systems, we are often interested in long-time averaged quantities rather than instantaneous quantities. Furthermore, we want to perform sensitivity analysis, i.e. to know how the change in the parameters of the systems would affect those long-time averaged quantities. Such sensitivity analysis is the purpose of this paper.

Consider a deterministic dynamical system parameterized by s :

$$\frac{du}{dt} = f(u, s) \quad (1)$$

Here $f(u, s) : \mathbb{R}^m \times \mathbb{R} \rightarrow \mathbb{R}^m$ is a smooth function, u is the state. A solution $u(t)$ is called the primal solution. The initial condition of the primal solution is denoted by $u(t=0) = u_0$.

*Corresponding author.

Email addresses: niangxiu@mit.edu (Angxiu Ni), qiqi@mit.edu (Qiqi Wang)

Let $J(u, s) : \mathbb{R}^m \times \mathbb{R} \rightarrow \mathbb{R}$ be a continuous function which defines the instantaneous objective. The averaged J over a time period of T is:

$$\langle J \rangle_T := \frac{1}{T} \int_0^T J(u, s) dt \quad (2)$$

$\langle J \rangle_T$ is a function of s , u_0 , and T . If we let T goes to infinity, then we obtain $\langle J \rangle_\infty$, which is only determined by s and u_0 . Here we make the assumption of ergodicity [3], which means that u_0 does not affect $\langle J \rangle_\infty$. As a result, the objective we are interested in, $\langle J \rangle_\infty$, is only a function of s .

We are interested in computing the sensitivity $d \langle J \rangle_\infty / ds$, since it is useful information in helping scientists and engineers design products [4, 5], control processes and systems [6, 7], solve inverse problems [8], estimate simulation errors [9, 10, 11], assimilate measurement data [12, 13] and quantify uncertainties [14].

However, when the dynamical system is chaotic, computing a meaningful $d \langle J \rangle_\infty / ds$ is challenging. The conventional way includes finite difference method and the transient method, which applies conventional tangent method directly to chaotic systems. One of the new approaches is the ensemble method developed by Lea et al[15, 16]. It computes the sensitivity by averaging $d \langle J \rangle_T / ds$ over an ensemble of trajectories. Another recent approach is based on the fluctuation dissipation theorem (FDT)[17, 18, 19, 20, 21, 22].

This paper follows the approach of Least Square Shadowing (LSS) developed by Wang, Hu and Blonigan [23, 14]. LSS first computes a bounded shift of a trajectory under parameters change, which is called LSS solution. Then we can substitute the LSS solution into the derivative of equation 2 to compute $d \langle J \rangle_\infty / ds$. LSS has been successfully applied to some dynamical systems such as the Lorenz 63 system and a modified Kuramoto-Sivashinsky equation[24, 14, 25]. LSS has also been applied by Blonigan et al. to engineering applications such as sensitivity analysis for airfoils[26, 25]. It has been proved by Wang that under ergodicity and hyperbolicity assumptions, LSS converges to the correct sensitivity at a rate of $T^{-0.5}$, where T is the trajectory time length[23].

However, for very large systems, LSS is still expensive; it is also not very easy to implement. In the original formulation of LSS, the majority of computation comes from solving a least square problem by its KKT conditions. After taking Schur complement, the number of variables in the linear equation system is the product of the dimension of the system, m , and the number of total time steps, N . The matrix of the equation system is tridiagonal and the main diagonal blocks are dense; the number of non-zero elements are about $m^2 N$. As the system gets larger and trajectory longer, the linear equation system becomes very large, and perhaps stiff as well. Although preconditioning and iterative solvers can accelerate solving this equation system [25], it would still be a large cost in both computer time and computer memory. Furthermore, previous formulations of LSS are intrusive, requiring Jacobian matrix $\partial_u f(u, s)$ at each time step. However, many existing simulation software may not readily provide such information, thus requiring modification to the code.

The Non-Intrusive Least Square Shadowing (NILSS) is relatively faster and easier to use than the conventional LSS method. The cost of NILSS is roughly proportional to the dimension of the attractor, which is much lower than the dimension of the system for many engineering applications. Hence NILSS could be much cheaper to solve under this scenario. Another benefit is that the information required in NILSS can be obtained without intrusive modification to existing tangent solvers, since NILSS no longer requires $\partial_u f(u, s)$. NILSS does require the underlying tangent solver being able to do numerical integration starting from any initial condition, whereas most existing solvers are coded only to perform integration from zero initial condition. Nevertheless, it greatly reduces the amount of intruding, which could encourage more engineers to use this method. Also, NILSS needs to store less data than the conventional LSS. Furthermore, the formulation of NILSS allows implementation which could put most of its data onto hard drive instead of computer memory.

The rest of this paper is organized as follows: First, we address the sensitivity with respect to parameters and initial conditions, and the relation between them. Then we explain tangent NILSS method. Then we present a more detailed flowchart of tangent NILSS algorithm on multiple time segments. Finally, we apply tangent NILSS to the Lorenz 63 system and a CFD simulation of a flow over a backward-facing step.

2. Sensitivity to initial conditions and parameters

Trajectories of chaotic dynamical systems depends sensitively on its parameters. Change the parameters of the governing equation by a small amount, the new trajectory will grow further apart from the old one, even though they start from the same initial condition. This is similar to the better known ‘butterfly effects’, which is the sensitive dependence on the initial condition. It means that for chaotic systems, a small difference in the initial condition can result in a large difference later on.

For example, the Lorenz 63 system is a simplified ODE model for atmospheric convection[27]. It has three state parameters x, y, z and a parameter ρ . In figure 1 we show the sensitive dependence of trajectories on both the initial condition and the parameter. For the left column, we plot on the x - z plane 1.8×10^7 trajectories with the same initial condition but different ρ . Here ρ is uniformly distributed between 27.999 and 28.001: smaller ρ is indicated by colors with shorter wavelength (blue), while larger ρ by longer wavelength (red). On the right column, we plot the same number of trajectories with the same parameter $\rho = 28$ but slightly different initial conditions u_0 .

As we can see in the first three pictures on the left, changing s has is similar to changing ρ : All these trajectories part from each other in a very similar way. Eventually, as shown in the last picture on the left, all trajectories settle into distribution similar to the attractor on the right. However, notice that the last figure on the left has different colors in different parts: the upper rim of is red, and the lower rim is blue. This is due to that the figure is the superposition of many attractors with different parameters. Red colors correspond to attractors

with a large ρ . So the red shade on the upper rim indicates that as we increase ρ , the attractor moves upward in the z direction. This means that $\langle z \rangle_\infty$ may have a positive and well-defined sensitivity with respect to ρ .

Hence changing ρ has two effects. In the short time, it results in diverging trajectories which looks exactly like only changing u_0 . In the long time, it results in a shifted attractor. The latter effect is hidden under the diverging trajectories and is only visible after a long time. However, it is the shift in the attractor that we want for computing the sensitivity. Our main goal in this paper, is to devise an algorithm such that we can ‘subtract’ the effect of changing u_0 from that of changing ρ , so that we can obtain the shift of the attractor. We will solidify above qualitative description in later sections.

3. Explanation of tangent NILSS

In this section we provide an explanation of tangent NILSS. First we describe the two effects of changing parameters, as described in the last section. Then we see why V^\perp , the subspaces perpendicular to f , has its own Lyapunov Characteristic Vectors (LCV). Then we see how NILSS formulate the desired tangent solution from 1) a particular tangent solution v^* , and 2) several homogeneous solutions $\{w_j\}$. Finally, we look at how to compute $d\langle J \rangle_\infty / ds$ from tangent solutions. Also, Appendix A explains the derivation of $d\langle J \rangle_\infty / ds$.

3.1. Two effects of a parameter perturbation

Assume the dynamical system in equation (1) has an infinitesimal perturbation Δs in the parameter, the new parameter is $s + \Delta s$. The new solution is denoted by $u + \Delta u$, which satisfy:

$$\frac{d(u + \Delta u)}{dt} = f(u + \Delta u, s + \Delta s)$$

Subtract by equation (1) and neglect second order small quantities. Let $v = \Delta u / \Delta s$, since Δs is infinitesimal, $v = du / ds$. v satisfies the following tangent equation:

$$\frac{dv}{dt} - \partial_u f v = \partial_s f \quad (3)$$

Here $\partial_u f$ is a $\mathbb{R}^m \times \mathbb{R}^m$ matrix and $\partial_s f$ is a \mathbb{R}^m column vector.

This v is undetermined unless a initial condition is specified. Conventionally, zero initial condition is used. We denote v^* as the solution of equation 3 with the initial condition $v^*(t = 0) = 0$. v^* is also the solution of conventional tangent method, its zero initial condition is due to that we assume u_0 is unchanged. Hence v^* characterizes the kind of perturbation in the left column of figure 1.

If there is a small perturbation in u_0 but no perturbation in s , the new solution satisfies:

$$\frac{du + \Delta u}{dt} = f(u + \Delta u, s)$$

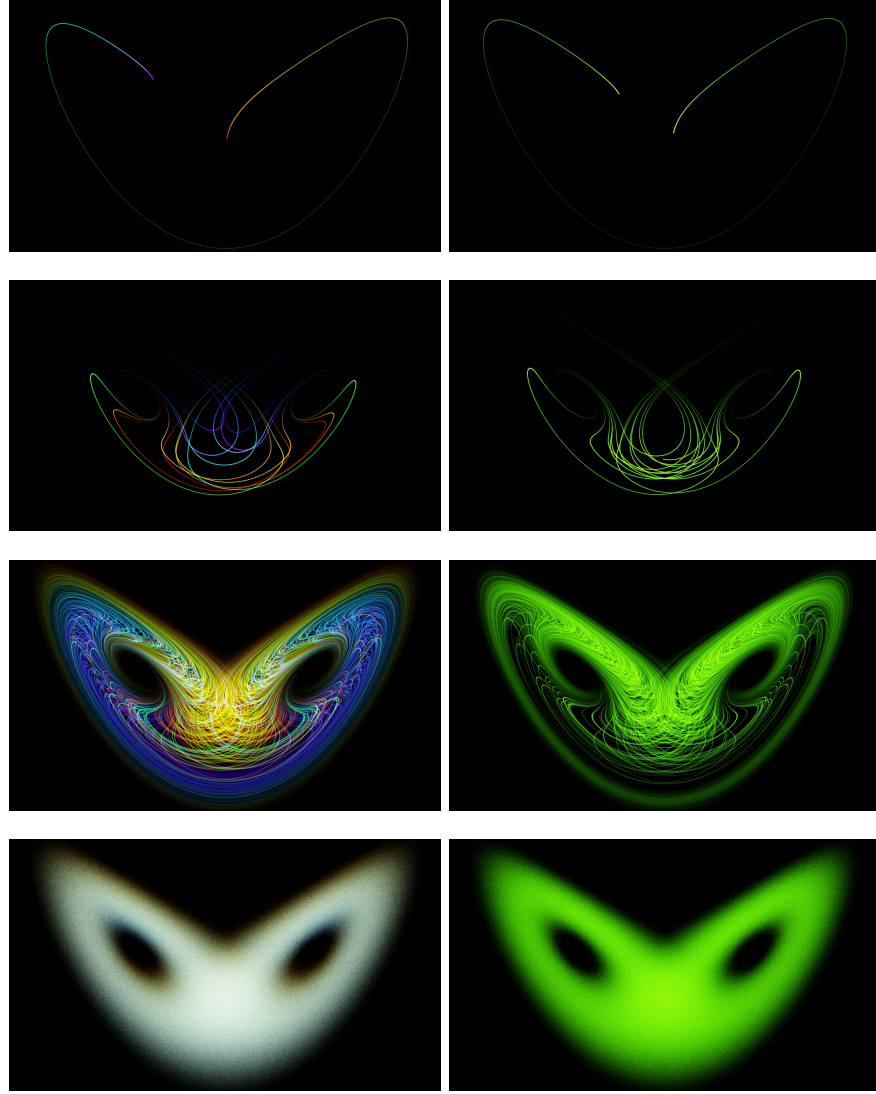


Figure 1: Sensitive dependence of trajectories on: initial value (left) and parameters of governing equations (right). Different colors indicate different parameter values.

Through the same deduction, denote $w = du/ds$, it satisfies the homogeneous tangent equation:

$$\frac{dw}{dt} - \partial_u f w = 0 \quad (4)$$

w characterizes the kind of perturbation in the right column of figure 1.

Hence v^* and w describe the effect of changing s and u_0 , respectively. Also, equation 4 differs from equation 3 by setting the right hand side to zero. If two different tangent solutions, say v^* and an arbitrary v , both satisfies equation 3, their difference is a homogeneous tangent solution w .

This matches our previous description: changing s has two effects, one is the same as changing u_0 , the other is shifting the attractor. Since we are interested in the latter, we want to find a w such that $v = v^* - w$ characterizes the motion of the attractor. In fact, subtracting such w from v^* is the main idea behind NILSS. The criterion of a correct v is that the magnitude of v^\perp is small, the reason for which is described in Appendix A.

Here v^\perp is defined through the orthogonal projection onto $V^\perp(u)$, the subspaces perpendicular to $f(u)$. This projection gives v^\perp , w^\perp , Δu^\perp , and $v^{*\perp}$, corresponding to v , w , Δu , and v^* . For example, v^\perp is:

$$v^\perp = v - \frac{f^T v}{f^T f} f$$

It is known by the shadowing lemma [28] that such a desired tangent solution v^∞ exists, but it is challenging to find. The main goal of NILSS is to find a w such that $v = v^* - w \approx v^\infty$. This could be easily done if we could know all Lyapunov Characteristic Vectors (LCV), which is the topic of the next subsection.

3.2. Decomposition of the perpendicular subspace V^\perp

NILSS and conventional LSS both assumes uniform hyperbolicity. But for the simplicity of discussion, we make a stronger assumption in this paper, that is, the dynamical system has a full set of Lyapunov Exponents (LE) and corresponding Lyapunov Characteristic Vectors (LCV). More specifically, there is $\{\lambda_j\}$, $j = 1, 2, \dots, m$, such that for all u on the attractor and homogeneous tangent solution w , there is a unique representation of w as:

$$w = \sum_{j=1}^m a_j(u) \zeta_j(u) \quad (5)$$

Here each $\zeta_j(u)$ is a homogeneous tangent solution, and its magnitude behaves like exponential functions of time. That is, there exists C_1 and C_2 , such that for any primal $u(\tau)$ on the attractor, for any j and t ,

$$C_1 e^{\lambda_j t} \|\zeta_j(u(0))\| \leq \|\zeta_j(u(t))\| \leq C_2 e^{\lambda_j t} \|\zeta_j(u(0))\| \quad (6)$$

This relation will also be denoted by:

$$\|\zeta_j(u(t))\| \approx e^{\lambda_j t} \|\zeta_j(u(0))\| \quad (7)$$

$\{\lambda_j\}$ and $\{\zeta_j\}$ are LEs and LCVs, respectively. LCVs with positive λ_j are called unstable modes, while those with negative λ_j is called stable modes. Unstable

modes are the reason for ‘butterfly effect’, since a perturbation in the unstable subspace grows exponentially in time.

We further assumes that there is only one zero LE, and its LCV is parallel to $f(u)$. We also require that all LCVs are uniformly bounded away from each other, that is, the angles between any two LCVs are bigger than some α_0 for all u on the attractor.

Notice that stable and unstable modes are not necessarily in V^\perp . However, we can project them onto V^\perp , to obtain a similar decomposition on $V^\perp(u)$. For any $w^\perp \in V^\perp(u)$,

$$w^\perp = \sum_{j=1}^m a_j(u) \zeta_j^\perp(u) \quad (8)$$

where $\zeta_j^\perp(u)$ are orthogonal projection of $\zeta_j(u)$ onto $V^\perp(u)$. We also call ζ_j^\perp stable or unstable modes based on their corresponding λ_j .

Since angles between $\{\zeta_j\}$ and $f(u)$ are greater than α_0 , the angles between $\{\zeta_j^\perp\}$ and V^\perp are always smaller than $\pi/2 - \alpha_0$. This means the amplitude of $\{\zeta_j^\perp\}$ still behaves like exponentials:

$$\|\zeta_j^\perp(u(t))\| \approx e^{\lambda_j t} \|\zeta_j^\perp(u(0))\| \quad (9)$$

Notice there are $(m-1)$ such ζ_j^\perp since $V^\perp(u)$ is a $(m-1)$ dimensional space. Their corresponding λ_j are all non-zero.

The analytical solution has non-zero initial condition $v^\infty(0) \neq 0$, however, conventional tangent solution uses zero initial condition $v^*(0) = 0$. The difference between the two initial conditions very likely contains some unstable components. This causes the exponential growth in the magnitude of v^* and $v^{*\perp}$, and the computation failure in the transient method.

Assume that we know each unstable ζ_j^\perp , we can subtract from $v^{*\perp}$ its projection onto each of them. Denote this result by $v^{L\perp}$, then $v^{L\perp} - v^{\infty\perp}$ do not have significant unstable modes. In other words, their difference is mainly stable modes, which decays very fast. v^L obtained in this way satisfies the criterion that $v^{L\perp}$ is small, and can be used to compute sensitivity.

To achieve the same effect, we only need to know the span of unstable modes, instead of knowing each of them separately. Moreover, subtracting ζ_j^\perp from $v^{*\perp}$ is the same as find the closest point in the affine space $v^{*\perp} + \text{span}\{\zeta_j^\perp\}$ to the origin. This leads to NILSS method.

3.3. Computing bounded v^\perp by NILSS

This subsection presents the main part of NILSS, that is, how to find a v^\perp whose magnitude is as small as possible.

To do this, we minimize the L^2 norm of $v^{N\perp} = v^{*\perp} + W^\perp a$:

$$\min_a \frac{1}{2} \int_0^T (v^{*\perp} + W^\perp a)^T (v^{*\perp} + W^\perp a) \quad (10)$$

Here $W^\perp(t) = \{w_j^\perp(t), j = 1, \dots, M\}$. The initial condition $w_j(t = 0)$ are randomized bounded vector in \mathbb{R}^m . The arguments for the optimization problem, a , is a column vector in \mathbb{R}^p .

Here M is an integer larger than the number of positive LEs. In the paper about computing LEs [29], we can see that $\text{span}\{w_j^\perp\}$ approximately contains the span of unstable modes. Due to the arguments in last subsection, we know that there exists an a which could give a desired v^L . Furthermore, due to the minimization, the magnitude of v^\perp is even smaller than v^L . Hence the result v can be used to compute sensitivity. The formalized argument of why v^* approximates v^* is beyond the scope of this paper, and it will appear in a different paper.

In the minimization of $\|v^{N\perp}\|$, the unstable modes in the error will be suppressed since their magnitudes grow exponentially. On the other hand, the minimization might introduce additional components in stable modes. However, stable modes will decay exponentially hence their impact on the magnitude of v is negligible. The intuition of the effect of minimization is illustrated in Figure 2.

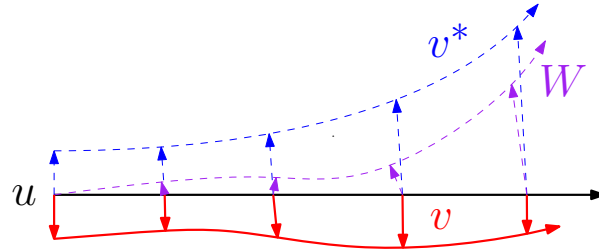


Figure 2: $v^\perp = v^{*\perp} + W^\perp a$, want to find a v^\perp whose magnitude is small.

There are only M arguments in the minimization problem posed in equation 10, hence the optimization problem in NILSS is very cheap to solve. On the other hand, the main cost in NILSS is in preparing the optimization problem, that is, to compute $v^{*\perp}$ and $w_1^\perp(t), \dots, w_M^\perp(t)$. For problems with a low dimensional attractor, there are fewer unstable modes, hence fewer $\{w_j\}$ to compute. As a result, NILSS has lower cost.

A beneficial side-effect is that the total amount of data we need to store is less than that of the conventional LSS method. Furthermore, all the tangent solutions used in NILSS need not be put into computer memory at the same time. The formulation of NILSS allows us to put those tangent solutions on hard drive, and read in two tangent solutions sequentially to compute their inner product. This implementation may reduce the computation speed, but saves much computer memory. Also, the optimization problem in equation 10 is very small and requires little memory. To summarize, NILSS could potentially require much less computer memory than conventional LSS.

3.4. Compute $d\langle J \rangle_\infty/ds$ from the tangent solution

Since $v - v^\perp$ is parallel to f , we can define

$$\xi f = v - v^\perp \quad (11)$$

To find a pair (v^\perp, ξ) , first solve equation 3 to get v , project v onto subspace V^\perp to find v^\perp , then use equation 11 to find ξ .

Once we obtain a v^N such that the magnitude of $v^{N\perp}$ is small, we can compute corresponding ξ^N . Then we have the following approximation for $d\langle J \rangle_\infty/ds$:

$$\frac{d\langle J \rangle_\infty}{ds} \approx \frac{1}{T} \left[\int_0^T (\partial_u f v^N + \partial_s J) dt + \xi|_0^T \langle J \rangle_T - (\xi J)|_0^T \right] \quad (12)$$

Here $\langle J \rangle_T$ is as defined in equation 2. Explanation of the above formula is in Appendix A.

4. Tangent NILSS Algorithm

In this section, first we talk about how to avoid $v^{*\perp}$ and W^\perp from becoming too large, by rescaling them after every short segment of time ΔT . Then we discuss the criterion for determining the number of homogeneous solutions, M , and segment length, ΔT . Finally, we provide a detailed walk-through of the tangent NILSS algorithm.

A variation of tangent NILSS is the finite difference NILSS. This formulation is obtained by approximating the tangent solutions by finite difference solutions. An explanation of finite difference NILSS could be found in Appendix B.¹

4.1. Solving NILSS on multiple time segments

Since both $v^{*\perp}$ and W^\perp grow exponentially, the round off error will soon become non-negligible. It will also make the covariance matrix $(W^\perp)^T W^\perp$ singular, since all w_j^\perp will eventually be dominated by the fastest growing unstable direction. This subsection shows how to prevent this by partitioning a long trajectory into several shorter segments.

Partition the time domain into K time segments $[t_0, t_1], [t_1, t_2], \dots, [t_{K-1}, t_K]$, with $t_0 = 0, t_K = T$. Define time segment i as $[t_i, t_{i+1}], i = 0, \dots, K-1$. Then $v^{*\perp}$ and W^\perp become $\{v_i^{*\perp}\}$ and $\{W_i^\perp\}$ for time segment i . Above notations is also depicted in Figure 3.

We want to rescale $v^{*\perp}$ and W^\perp at the end of each segment so that they do not grow too large. We also want to keep the affine vector space $v^{*\perp} + \text{span}(W^\perp)$ the same across these segments.:

$$v_i^{*\perp}(t_i) + \text{span}(W_i^\perp(t_i)) = v_{i-1}^{*\perp}(t_i) + \text{span}(W_{i-1}^\perp(t_i)) \quad (13)$$

¹The python code that implemented the algorithm introduced in this paper, both tangent NILSS and the finite difference variant, are available at github.com/qiqi/fds.

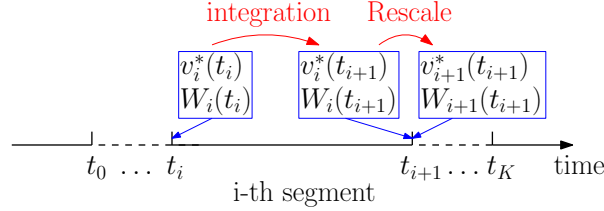


Figure 3: Notations used for tangent NILSS, $t_0 = 0, t_K = T$

Where $\text{span}(W^\perp)$ is the vector space spanned by the column vectors of W^\perp .

To achieve this, first orthonormalize W^\perp with a QR decomposition:

$$W_i^\perp(t_{i+1}) = Q_i R_i \quad (14)$$

set the initial conditions of the next tangent segment to

$$W_{i+1}^\perp(t_{i+1}) = Q_i \quad (15)$$

In QR factorization, the column vectors in Q_i and W_i^\perp could represent each other. Hence $\text{span}(W_i^\perp(t_i)) = \text{span}(W_{i-1}^\perp(t_i))$.

Then use Gram-Schmit for $v^{*\perp}$. That is, rescale $v^{*\perp}$ by subtracting its orthogonal projection on W^\perp to obtain the initial condition of the next time segment:

$$v_{i+1}^{*\perp}(t_{i+1}) = v_i^{*\perp}(t_{i+1}) - W_{i+1}^\perp(t_{i+1}) b_i$$

here $b_i = W_{i+1}^\perp(t_{i+1})^T v_i^{*\perp}(t_{i+1})$. Notice that $v_{i+1}^{*\perp}(t_{i+1})$ is still in the affine space $v_i^{*\perp}(t_i) + \text{span}(W_i^\perp(t_i))$.

Now equation 13 is satisfied, for any a_{i-1} , there exists a_i such that:

$$v_i^{*\perp}(t_i) + W_i^\perp(t_i) a_i = v_{i-1}^{*\perp}(t_i) + W_{i-1}^\perp(t_i) a_{i-1}$$

Hence we can enforce the continuity requirement on $\{v_i^{N\perp}\}$:

$$v_i^{N\perp}(t_i) = v_{i-1}^{N\perp}(t_i) \quad (16)$$

Hence the solution v^N on multiple time segment is same as that of one longer segment. However, rescaling $v^{*\perp}$ and W^\perp at the end of each time segment prevents them from growing too large.

It is not a new idea of using QR factorization to rescale homogeneous solutions while keeping a continuous subspace. In the paper of computing LE [29], the same technique was used.

4.2. Determining parameters for NILSS

There are two parameters in NILSS for users to decide: number of homogeneous solutions and length each of time segments. This subsections briefly talks about how to determine these parameters.

LEs are a byproduct of NILSS, since our procedure of rescaling $\{w_j^\perp\}$ at the end of each time segment is exactly the same as that used in computing LEs [29]. To obtain the j -th largest LE, we just need to take average of the j -th diagonal element in R_i over all $i = 0, 1, \dots, K-1$. In practice, we can gradually increase the number of homogeneous solutions until all positive LEs show up. Then we select M bigger than the number of positive LEs.

On the other hand, we want to partition the whole trajectory so that the LCV with the largest LE do not dominate the M -th LCV. Otherwise the covariance matrix grows singular, since all $\{w_j^\perp\}$ will be almost parallel to the LCV with largest LE. Assume the largest LE is λ_{\max} , and M -th LE is λ_M . We want to rescale W^\perp and $v^{*\perp}$ after time span $\Delta T \leq (\lambda_{\max} - \lambda_M)^{-1}$. This relation determines how we select ΔT . Note that in general $\lambda_{\min+} \neq \lambda_M$.

4.3. Pre-process

From here on we look at the detailed algorithm of NILSS.

Fist integrate equation (1) for some time, and then set $t = 0$, so that u is on the attractor at the beginning of our algorithm. Next, integrate equation (1) from $t = 0$ to T , to obtain the primal solution $u(t)$.

4.4. Compute the homogeneous solution $\{W_i\}$

We solve M tangent equations on each of the K time segments $[t_0, t_1], \dots, [t_{K-1}, t_K]$, with $t_0 = 0, t_K = T$. Time segment i is the time span $[t_i, t_{i+1}]$. This notation is the same as that in Figure 3.

We start at the first time segment with random initial conditions $W_0(0) = [w_{0,1}(0), \dots, w_{0,p}(0)]$, where $w_{0,j}(0) \in V^\perp(u(0))$. Then proceed with the following algorithm starting at $i = 0$.

1. Starting from the initial conditions

$$W_i(t_i) = [w_{i,1}(t_i), \dots, w_{i,M}(t_i)],$$

integrate the homogeneous equations to obtain

$$W_i(t_{i+1}) = [w_{i,1}(t_{i+1}), \dots, w_{i,M}(t_{i+1})].$$

2. Computes the orthogonal projection onto V^\perp :

$$W_i^\perp = [w_{i,1}^\perp, \dots, w_{i,M}^\perp],$$

Meanwhile, compute and store

$$C_i = \int_{t_i}^{t_{i+1}} (W_i^\perp)^T W_i^\perp dt.$$

3. Orthonormalize $W_i^\perp(t_{i+1})$ with a QR decomposition:

$$W_i^\perp(t_{i+1}) = Q_i R_i.$$

R_i and Q_i can also be computed through Cholesky decomposition of $W_i^\perp(t_{i+1})^T W_i^\perp(t_{i+1})$. Store R_i and set the initial conditions of the next tangent segment to

$$W_{i+1}(t_{i+1}) = Q_i.$$

4. Let $i = i + 1$. Go to Step 1 unless i is greater than $K - 1$, in which case the algorithm terminates.

4.5. Compute the inhomogeneous solution $\{v_i^*\}$

We start at the first time segment with a zero initial condition $v_0^*(0) = 0$. Proceed with the following algorithm starting at $i = 0$.

1. Starting from the initial condition $v_i^*(t_i)$, integrate the inhomogeneous equations to obtain $v_i^*(t_{i+1})$. Then compute the orthogonal projection, $v_i^{*\perp}$. Meanwhile, compute and store

$$d_i = \int_{t_i}^{t_{i+1}} W_i^\perp{}^T v_i^{*\perp} dt,$$

2. Orthogonalize $v_i^{*\perp}(t_{i+1})$ with respect to $W_{i+1}^\perp(t_{i+1})$ via Gram-Schmidt procedure to obtain the initial condition of the next time segment:

$$v_{i+1}^*(t_{i+1}) = v_i^{*\perp}(t_{i+1}) - W_{i+1}^\perp(t_{i+1})b_i$$

where

$$b_i = W_{i+1}^\perp(t_{i+1})^T v_i^{*\perp}(t_{i+1})$$

should be stored.

3. Let $i = i + 1$. Go to Step 1 unless i is greater than $K - 1$, for which case the algorithm terminates.

Here we present solving inhomogeneous solution v_i^* as a separate step after the homogeneous solution W_i . They can also be integrated simultaneously.

4.6. Compute the NILSS tangent, v^N

The arguments of the minimization problem in tangent NILSS are $a_i \in \mathbb{R}^M, i = 0, \dots, K - 1$. The minimum norm statement is now minimizing

$$\sum_{i=0}^{K-1} \int_{t_i}^{t_{i+1}} [(v_i^{*\perp})^T v_i^{*\perp} + 2(v_i^{*\perp})^T W_i^\perp a_i + a_i^T (W_i^\perp)^T W_i^\perp a_i] dt$$

Other than a constant contribution from $(v_i^{*\perp})^T v_i^{*\perp}$, we should choose a_i 's as

$$\min_{\{a_i\}} \sum_{i=0}^{K-1} 2d_i^T a_i + a_i^T C_i a_i. \quad (17)$$

The continuity of $v^{N\perp}$ across t_i can be written as

$$v_{i-1}^{*\perp}(t_i) + W_{i-1}^\perp(t_i)a_{i-1} = v_i^{*\perp}(t_i) + W_i^\perp(t_i)a_i$$

Consider the relationship of $v_{i-1}^{*\perp}$ to $v_i^{*\perp}$ and W_{i-1}^\perp to W_i^\perp at t_i , the above continuity requirement transforms into:

$$v_i^{*\perp}(t_i) + W_i^\perp(t_i)b_{i-1} + W_i^\perp(t_i)R_{i-1}a_{i-1} = v_{i-1}^{*\perp}(t_i) + W_{i-1}^\perp(t_i)a_i$$

Which is equivalent to:

$$a_i = R_{i-1}a_{i-1} + b_{i-1} \quad (18)$$

Combining the minimization problem in equation (17) and the continuity constraints in equation (18), we obtain the constraint least squares problem:

$$\begin{aligned} \min_{\{a_i\}} \sum_{i=0}^{K-1} 2d_i^T a_i + a_i^T C_i a_i \\ \text{s.t. } a_i = R_{i-1}a_{i-1} + b_{i-1} \quad i = 1, \dots, K-1, \end{aligned} \quad (19)$$

Once $\{a_i\}$ is obtained by solving equation (19), we can compute v_i^N within each time interval $t \in [t_i, t_{i+1}]$ by:

$$v_i^N(t) = v_i^*(t) + W_i(t)a_i \quad (20)$$

Notice that here v_i^N is not continuous across the t_i , but $v_i^{N\perp}$ is. The number of arguments in this minimization problem is $M \times K$, which is smaller than conventional LSS.

4.7. Compute ξ_i

At the beginning of each segment, v^* and W are in V^\perp , hence so is v^N . As a result,

$$\begin{aligned} \xi_i(t_i) &= 0 \\ \xi_i(t_{i+1}) &= \frac{(v_i^N(t_{i+1}))^T f(u(t_{i+1}))}{f(u(t_{i+1}))^T f(u(t_{i+1}))} f(u(t_{i+1})) \end{aligned} \quad (21)$$

4.8. Compute $d\langle J \rangle / ds$

Once $v^N(t)$ is obtained, $d\langle J \rangle_\infty / ds$ is computed by

$$\frac{1}{T} \sum_{i=0}^{K-1} \int_{t_i}^{t_{i+1}} (\partial_u f v_i^N + \partial_s J) dt + \xi_i(t_{i+1})(\langle J \rangle_T - J(T)) \quad (22)$$

To derive equation 22 from equation 12, notice that a continuous ξ could be recovered by ‘accumulating’ all previous ξ_i , that is:

$$\xi(t) = \xi_i(t) + \sum_{i'=0}^{i-1} \xi_{i'}(t_{i'+1}), \quad t \in [t_i, t_{i+1}]$$

Alternatively, the sensitivity can be computed without explicitly forming $v^N(t)$. The sensitivity contribution of v^N within each time interval can be computed from v_i^* and $w_{i,j}$ when they are solved, and a linear combination of them, with a_i being the coefficients.

5. Numerical Results on Lorenz attractor

We apply the tangent NILSS to the Lorenz 63 system. It has three states, that is, $m = 3$, and the governing equation is:

$$\frac{dx}{dt} = \sigma(y - x), \quad \frac{dy}{dt} = x(\rho - z) - y, \quad \frac{dz}{dt} = xy - \beta z \quad (23)$$

In our current numerical example, we set $\sigma = 10, \beta = 8/3$.

The parameter of the system is ρ , which varies in range [2, 45]. The Lorenz 63 system has different behaviors when ρ changes [30]:

- $2 \leq \rho < 24.7$, two stable point attractors.
- $24.7 \leq \rho < 31$, one quasi-hyperbolic strange attractor.
- $31 \leq \rho \leq 45$, one non-hyperbolic attractor.

For our study, we select the quantity of interest to be:

$$\langle J \rangle = \lim_{T \rightarrow \infty} \frac{1}{T} \int_0^T z \, dt$$

When solving the primal solution $u = (x, y, z)^T$, we use Euler forward integration with time step size 0.005. Each segment has 1000 steps, that is, 5 time units. We perform NILSS over $K = 20$ segments.

It is known that the LEs of Lorenz 63 system should satisfy the following constraints [31]:

$$\begin{aligned} \lambda_1 + \lambda_2 + \lambda_3 &= -(1 + \sigma + \beta) \\ \lambda_2 &= 0 \end{aligned}$$

Here λ_2 is the LE whose corresponding LCV is parallel to du/dt . Since $\lambda_1 + \lambda_3 < 0$, there are at most 1 positive LE. Hence we set the number of homogeneous solutions to be $M = 1$.

With above setting, we compute $\langle J \rangle_T$ and $d\langle J \rangle_\infty / d\rho$. The result is shown in figure 4 and figure 5. It can be observed from figure 4 that the true value of $\frac{d\langle J \rangle}{d\rho}$ is about 1 for all ρ . The sensitivities computed with NILSS match this observation.

6. Numerical Results on CFD Simulation of flow over a backward-facing step

We apply NILSS to a chaotic flow over a backward-facing step. Specifically, we use same geometry and mesh as in the PitzDaily tutorial of OpenFOAM 4.0, which is modeled from the experiment by Pitz and Daily [32]. This problem is a two dimensional flow over a backward-facing step near the inlet and a contracting nozzle at the outlet. The geometry is shown in figure 6.

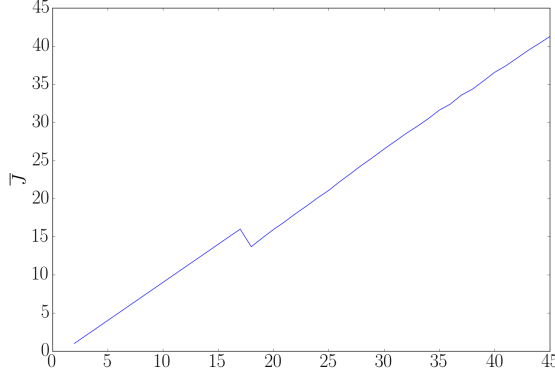


Figure 4: $\langle J \rangle$ computed for each ρ , averaged over 100 time units.

For the numerical simulation, we use OpenFOAM 4.0 as the solver. We use the mesh as provided in the tutorial, there are 12225 cells, which is shown in figure 7. Specifically, we solve incompressible Navier-Stokes equation by pisoFOAM. We use 2nd order finite volume scheme; the time-integration method is PISO (Pressure Implicit with Splitting of Operator), time step size is 1×10^{-5} second.

In terms of boundary conditions, we set no-slip wall condition for all boundaries except for the inlet and outlet. The inlet boundary takes a uniform fixed value in the x-direction, the magnitude of which is the parameter of this problem. For the base case, we set inlet velocity $U = (10, 0, 0)m/s$. For the outlet, we use the ‘inletOutlet’ option, which is to switch between the fixed value and the zero gradient boundary condition, depending on the flow direction.

With above settings, A typical snapshot of the flow field is shown in figure 8. The flow is chaotic but not turbulent, since it is two dimensional.

The parameter in this problem is the x-directional velocity at the inlet, U_{x0} . We use four different objectives: the long time average of U_x/U_{x0} , $(U_x/U_{x0})^2$, $(U_x/U_{x0})^4$, and $(U_x/U_{x0})^8$. Here U_x is the x-direction velocity at a probe at coordinate (50.8mm, 25.3mm). The location of the probe is very close to the upper surface, as shown in figure 8.

The objective $\langle J \rangle_T$ is averaged over 2×10^5 time steps, that is, $T = 2$ seconds. To get the uncertainty of the objective, we divide the simulation into 5 equally long parts, and average the objective over each part. Denote these averaged objectives by J_1, \dots, J_5 , the corrected sample standard deviation between them are:

$$\sigma' = \sqrt{\frac{1}{4} \sum_{k=1}^5 (J_k - \langle J \rangle_T)^2}$$

Here we assume that the standard deviation is proportional to $T^{-0.5}$, so we use

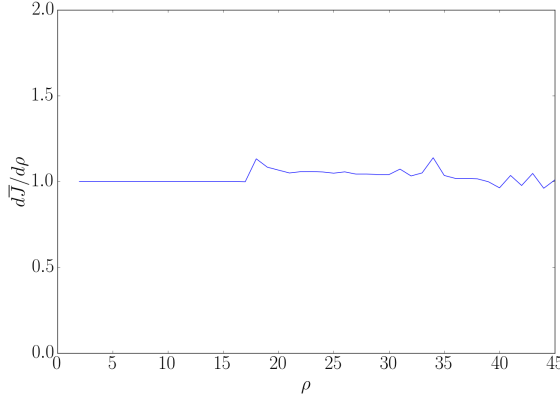


Figure 5: $\frac{d\langle J \rangle}{d\rho}$ computed for each ρ using tangent NILSS. The time length of trajectories is $T = 100$, and the whole time span is partitioned into 20 segments of length 5.



Figure 6: Geometry of the test case, dimensions in mm. All boundaries except inlet/outlet are solid walls.

$\sigma = \sigma'/\sqrt{5}$ as the standard deviation of $\langle J \rangle_T$. We further assume that, when averaging over random trajectories, the distribution of $\langle J \rangle_T$ is Gaussian, hence $\pm 2\sigma$ gives its 95% confidence interval. Objectives for difference parameters in range [9,11] are shown in the right column of figure 10, where the bars indicate the 95% confidence interval.

For NILSS, we use finite difference to approximate tangent solutions, as explained in Appendix B. Each segment has 250 time steps, that is, 0.0025 second. To compute the sensitivity, we run NILSS over $K = 200$ segments.

To determine number of homogeneous solutions, M , used in NILSS, we compute LEs by the method described in section 4.2. The value of an LE, denoted by λ , changes with T , or equivalently, the number of segments. We use λ_i to denote the value of this LE, computed using data from segments 1, 2, ..., i . Here we assume that $\{\lambda_i\}$ converges to some λ_0 as we increase i , and its confidence

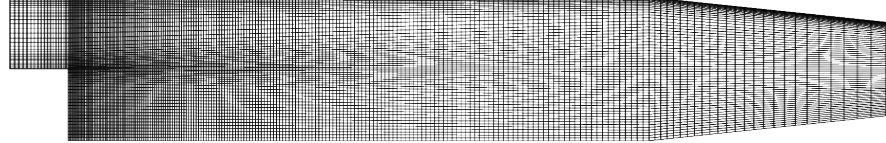


Figure 7: Mesh of test case

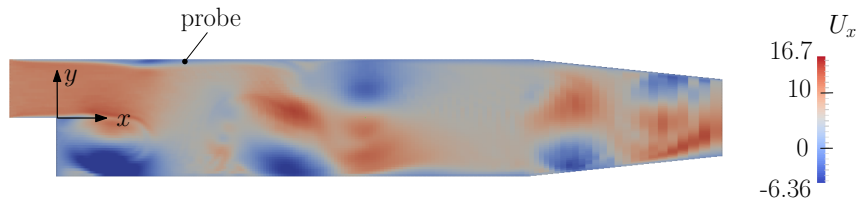


Figure 8: U_x at time 0.091

interval is proportional to $i^{-0.5}$. To find λ_0 , first define $C(\lambda_0)$ as:

$$C = \min\{C' \mid |\lambda_0 - \lambda_i| \leq C'i^{-0.5}, \text{ for all } i \leq K\}$$

Here K is the number of segments. We define λ_0 as such that the corresponding $C(\lambda_0)$ is smallest:

$$\lambda_0 = \arg \min_{\lambda} \{C(\lambda)\}$$

We regard $CK^{-0.5}$ as the confidence interval for λ_0 . The convergence history of the largest 16 LEs in semi-log coordinates are shown in the left of figure 9. The λ_0 and confidence intervals for each LE are shown in the right of figure 9. As can be observed, the total number of positive LEs is smaller than 16. So we set $M = 16$.

With above settings, the cost of NILSS is proportional to the total time steps computed, which is $200 \times 250 \times 18 = 9 \times 10^5$. Here 18 is the number of trajectories computed. We need one v^* and 16 $\{w_j\}$, that is 17 tangent solutions in total. Each tangent solution requires the finite difference between a base solution and a perturbed solution to approximate. These finite differences uses the same base solution, so we need to compute one base solution and 17 perturbed solutions. This means we need to compute 18 trajectories, each with 200×250 time steps in primal solution.

We want to give confidence intervals for the sensitivities computed by NILSS. Similar to the case of LE, the value of dJ/ds changes with T , or equivalently, the number of segments. We use $(dJ/ds)_i$ to denote the sensitivity computed using data from segments 1, 2, ..., i . Here we assume that $\{(dJ/ds)_i\}$ converges to some $(dJ/ds)_0$ as we increase i , and its confidence interval is proportional to

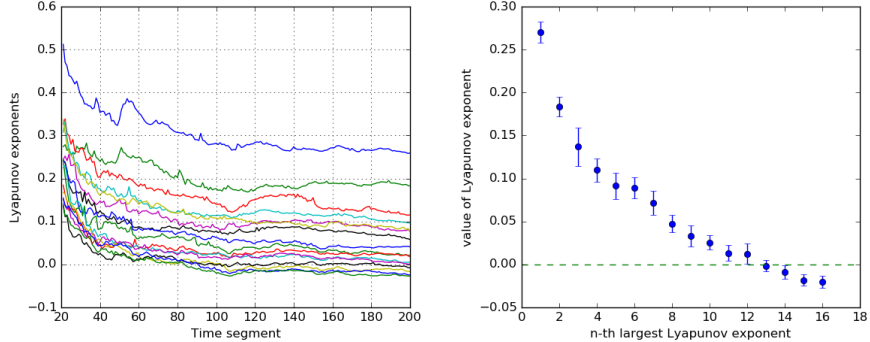


Figure 9: Lyapunov exponents (LE). Left: convergence history of LE. Right: confidence interval of the largest 16 LEs.

$i^{-0.5}$. To find $(dJ/ds)_0$, first define $C((dJ/ds)_0)$ as:

$$C = \min\{C' \mid |(dJ/ds)_0 - (dJ/ds)_i| \leq C'i^{-0.5}, \text{ for all } i \leq K\}$$

Here K is the number of segments. We define $(dJ/ds)_0$ as such that the corresponding $C((dJ/ds)_0)$ is smallest:

$$(dJ/ds)_0 = \arg \min_{dJ/ds} \{C(dJ/ds)\}$$

We regard $CK^{-0.5}$ as the confidence interval for $(dJ/ds)_0$. The left column in figure 10 is a log-log plot of $|(dJ/ds)_0 - (dJ/ds)_i|$ for $U_{x0} = 10$, where the lines indicate $Ci^{-0.5}$. Similarly, we find the confidence interval of the sensitivity at $U_{x0} = 11$. In the right column of figure 10, the wedges indicate these confidence intervals of sensitivities. As we can see, the sensitivities computed by NILSS correctly reflect the trend in long-time averaged objectives.

In our current example, the cost of the NILSS is roughly the same as that of the conventional finite difference method. For conventional finite difference method, we do a linear regression of the objectives over 5 parameters ranges in $[9,11]$; the total number of time steps computed in primal solutions is $5 \times 2 \times 10^5 = 1 \times 10^6$. In NILSS, the total number of time steps in primal solutions is 9×10^5 . This forms the major cost of finite difference NILSS, which is to approximate tangent solutions by finite difference. Hence, the total cost of NILSS is roughly the same as that of the conventional finite difference method.

However, here we are making a comparison in favor of the conventional finite difference. In figure 10, the range of parameters is 2. For the last two objectives, this range is too large, since the relations between objectives and parameters are not linear for parameters in the range $[9,11]$. In these cases, if we want to reduce the error in linearly approximating a nonlinear function, the parameters range should be smaller. However, this requires the confidence intervals of objectives also be reduced. Otherwise, the difference between objectives may have previous

magnitude of uncertainty, but is divided by a smaller parameter range to get the sensitivity; this would give rise to a large uncertainty in the sensitivity. To obtain smaller confidence intervals of objectives, we require longer trajectories, which means larger computational cost for the conventional finite difference method.

When there are multiple parameters, the cost of NILSS is even lower than conventional finite difference method. For tangent NILSS, equation 3 has right hand side $\partial_s f$, which says v^* would change if we have a new parameter. However, w_j does not depend on s , so they could be reused for the new parameter. The marginal cost for a new parameter is to solve for a new v^* . In our finite difference NILSS for this problem, 18 trajectories were computed, one is base trajectory, one is with perturbed parameter but same initial condition, 16 are with perturbed initial condition but same parameter. Only the one with perturbed parameter should be recomputed for a new choice of parameter. So the marginal cost of another parameter is only $1/18$ of the cost of the first parameter. On the other hand, for conventional finite difference, 5 trajectories are computed, one is base trajectory, 4 are with perturbed parameters. As a result, 4 trajectories should be recomputed for a new choice of parameter. This means the marginal cost of another parameter is $4/5$ of the cost of the first parameter, which is higher than that of finite difference NILSS.

The cost of the conventional LSS method is larger than NILSS. The number of states in our problem is $12225 \times 3 = 36675$. If we perform conventional LSS on a same time span of $200 \times 250 = 5 \times 10^4$ steps, the conventional LSS method would require solving a linear equation system whose matrix has about $36675^2 \times 5 \times 10^4 \approx 6.7 \times 10^{13}$ non zero elements. This would be a very large cost in both computation time and computer memory.

7. Conclusions

The Non-Intrusive Least Square Shadowing (NILSS) is a method which computes the sensitivity of long-time averaged objectives in chaotic systems. NILSS is a variant of the Least Square Shadowing (LSS) method [14], but it has several advantages over the conventional LSS method:

1. It potentially requires only minor modifications to existing tangent solvers.
2. For problems with a low dimensional attractor, which is the case for many engineering applications, NILSS has lower computational cost.
3. NILSS requires less computer memory.

NILSS has been demonstrated on the Lorenz 63 system and a CFD simulation for a flow over a backward-facing step. In both cases, the sensitivities given by NILSS can reflect the trend between objectives and parameters. For the latter case, NILSS has similar computational cost as the conventional finite difference method. We further argued that NILSS would be cheaper than the conventional finite difference, if the relation between objectives and parameters

is more nonlinear, or if we are interested in multiple parameters. It is also verified that the latter test case has a low-dimensional attractor, with less than 16 positive Lyapunov exponents.

References

References

- [1] A. N. Kolmogorov, The Local Structure of Turbulence in Incompressible Viscous Fluid for Very Large Reynolds Numbers, *Proceedings: Mathematical and Physical Sciences* 434 (1890) (1991) 9–13.
URL <http://www.jstor.org/stable/51980>
- [2] E. Dowell, Flutter of a buckled plate as an example of chaotic motion of a deterministic autonomous system, *Journal of Sound and Vibration* (1982) 333–344.
URL <http://www.sciencedirect.com/science/article/pii/0022460X82902590>
- [3] P. Walters, *An introduction to ergodic theory*, Vol. 79, Springer Science & Business Media, 2000.
- [4] A. Jameson, Aerodynamic design via control theory, *Journal of scientific computing* 3 (3) (1988) 233–260.
- [5] J. J. Reuther, A. Jameson, J. J. Alonso, M. J. Rimlinger, D. Saunders, Constrained Multipoint Aerodynamic Shape Optimization Using an Adjoint Formulation and Parallel Computers, Part 2, *Journal of Aircraft* 36 (1) (1999) 61–74. doi:10.2514/2.2414.
URL <http://arc.aiaa.org/doi/abs/10.2514/2.2414>
- [6] T. R. Bewley, Flow control: new challenges for a new Renaissance, *Progress in Aerospace Sciences* 37 (2001) 21–58.
URL <http://turbulence.ucsd.edu>.
- [7] T. R. Bewley, P. Moin, R. Temam, DNS-based predictive control of turbulence: an optimal benchmark for feedback algorithms, *Journal of Fluid Mechanics* 447 (2001) 179–225. doi:10.1017/S0022112001005821.
- [8] J. Tromp, C. Tape, Q. Liu, Seismic tomography, adjoint methods, time reversal and banana-doughnut kernels, *Geophys. J. Int.* doi:10.1111/j.1365-246X.2004.02453.x.
- [9] R. Becker, R. Rannacher, An optimal control approach to a posteriori error estimation in finite element methods, *Acta Numerica* 10. doi:10.1017/S0962492901000010.
URL http://www.journals.cambridge.org/abstract_S0962492901000010

[10] M. B. Giles, E. Süli, Adjoint methods for PDEs: a posteriori error analysis and postprocessing by duality, *Acta Numerica* 11. doi:10.1017/S096249290200003X.
 URL http://www.journals.cambridge.org/abstract_S096249290200003X

[11] K. J. Fidkowski, D. L. Darmofal, Review of Output-Based Error Estimation and Mesh Adaptation in Computational Fluid Dynamics doi:10.2514/1.J050073.

[12] J.-N. Thepaut, P. Courtier, Four-dimensional variational data assimilation using the adjoint of a multilevel primitive-equation model, *Quarterly Journal of the Royal Meteorological Society* 117 (502) (1991) 1225–1254. doi:10.1002/qj.49711750206.
 URL <http://doi.wiley.com/10.1002/qj.49711750206>

[13] P. Courtier, J. Derber, R. Errico, J. Louis, T. Vukićević, Important literature on the use of adjoint, variational methods and the Kalman filter in meteorology (oct 1993). doi:10.1034/j.1600-0870.1993.t01-4-00002.x.
 URL <http://tellusa.net/index.php/tellusa/article/view/14898> [http://onlinelibrary.wiley.com/doi/10.1034/j.1600-0870.1993.t01-4-00002.x/abstract\\$&delimit%20E30F&nhttp://www.blackwell-synergy.com/doi/abs/10.1034/j.1600-0870.1993.t01-4-00002.x](http://onlinelibrary.wiley.com/doi/10.1034/j.1600-0870.1993.t01-4-00002.x/abstract$&delimit%20E30F&nhttp://www.blackwell-synergy.com/doi/abs/10.1034/j.1600-0870.1993.t01-4-00002.x)

[14] Q. Wang, R. Hu, P. Blonigan, Least Squares Shadowing sensitivity analysis of chaotic limit cycle oscillations, *Journal of Computational Physics* 267 (2014) 210–224.

[15] D. J. Lea, M. R. Allen, T. W. N. Haine, Sensitivity analysis of the climate of a chaotic system, *Tellus Series a-Dynamic Meteorology and Oceanography* 52 (5) (2000) 523–532. doi:10.1256/qj.01.180.

[16] G. L. Eyink, T. W. N. Haine, D. J. Lea, Ruelle's linear response formula, ensemble adjoint schemes and Lévy flights, *Nonlinearity* 17 (5) (2004) 1867.

[17] J. Thuburn, Climate sensitivities via a FokkerPlanck adjoint approach, *Quarterly Journal of the Royal Meteorological Society* 131 (605) (2005) 73–92. doi:10.1256/qj.04.46.
 URL <http://doi.wiley.com/10.1256/qj.04.46>

[18] T. N. Palmer, A nonlinear dynamical perspective on model error: A proposal for non-local stochastic-dynamic parametrization in weather and climate prediction models, *Quarterly Journal of the Royal Meteorological Society* 127 (572) (2001) 279–304. doi:10.1002/qj.49712757202.
 URL <http://doi.wiley.com/10.1002/qj.49712757202>

[19] L.-S. Young, What are SRB measures, and which dynamical systems have them?, *Journal of Statistical Physics* 108 (5) (2002) 733–754.

[20] C. E. Leith, Climate Response and Fluctuation Dissipation, *Journal of the Atmospheric Sciences* 32 (10) (1975) 2022–2026. [doi:10.1175/1520-0469\(1975\)032<2022:CRAFD>2.0.CO;2](https://doi.org/10.1175/1520-0469(1975)032<2022:CRAFD>2.0.CO;2). URL <http://journals.ametsoc.org/doi/abs/10.1175/1520-0469%281975%29032%3C2022%3ACRAFD%3E2.0.CO%3B2>

[21] R. V. Abramov, A. J. Majda, Blended response algorithms for linear fluctuation-dissipation for complex nonlinear dynamical systems, *Nonlinearity* 20 (12) (2007) 2793.

[22] R. V. Abramov, A. J. Majda, New Approximations and Tests of Linear Fluctuation-Response for Chaotic Nonlinear Forced-Dissipative Dynamical Systems, *Journal of Nonlinear Science* 18 (3) (2008) 303–341. [doi:10.1007/s00332-007-9011-9](https://doi.org/10.1007/s00332-007-9011-9). URL <http://link.springer.com/10.1007/s00332-007-9011-9>

[23] Q. Wang, Convergence of the least squares shadowing method for computing derivative of ergodic averages, *SIAM Journal on Numerical Analysis* 52 (1) (2014) 156–170.

[24] P. Blonigan, S. Gomez, Q. Wang, Least Squares Shadowing for sensitivity analysis of turbulent fluid flows, in: 52nd Aerospace Sciences Meeting, 2014, pp. 1–24. [arXiv:1401.4163](https://arxiv.org/abs/1401.4163). URL <http://arxiv.org/abs/1401.4163>

[25] P. J. Blonigan, Least Squares Shadowing for Sensitivity Analysis of Large Chaotic Systems and Fluid Flows, Ph.d thesis, MIT (2016).

[26] P. J. Blonigan, Q. Wang, E. J. Nielsen, B. Diskin, Least Squares Shadowing Sensitivity Analysis of Chaotic Flow around a Two-Dimensional Airfoil, in: 54th AIAA Aerospace Sciences Meeting, no. January, 2016, pp. 1–28. [doi:10.2514/6.2016-0296](https://arc.aiaa.org/doi/10.2514/6.2016-0296). URL <http://arc.aiaa.org/doi/10.2514/6.2016-0296>

[27] E. N. Lorenz, Deterministic Nonperiodic Flow, *Journal of the Atmospheric Sciences* 20 (2) (1963) 130–141. [doi:10.1175/1520-0469\(1963\)020<0130:DNF>2.0.CO;2](https://doi.org/10.1175/1520-0469(1963)020<0130:DNF>2.0.CO;2). URL <http://journals.ametsoc.org/doi/abs/10.1175/1520-0469%281963%29020%3C0130%3ADNF%3E2.0.CO%3B2>

[28] S. Y. Pilyugin, Shadowing in Dynamical Systems, *Lecture Notes in Mathematics*. [doi:10.1007/BFb0093184](https://doi.org/10.1007/BFb0093184).

[29] G. Benettin, L. Galgani, A. Giorgilli, J.-M. Strelcyn, Lyapunov Characteristic Exponents for smooth dynamical systems and for hamiltonian systems; A method for computing all of them. Part 2: Numerical application, *Mecanica* 15 (1) (1980) 21–30. [doi:10.1007/BF02128237](https://doi.org/10.1007/BF02128237). URL <http://dx.doi.org/10.1007/BF02128237>

- [30] C. Sparrow, The Lorenz equations: bifurcations, chaos, and strange attractors, Vol. 41, Springer Science & Business Media, 2012.
- [31] J. Bovy, Lyapunov exponents and strange attractors in discrete and continuous dynamical systems, Tech. rep., KU Leuven University, Theoretical Physics Project (2004).
- [32] R. W. Pitz, J. Daily, Combustion in a turbulent mixing layer formed at a rearward facing step, AIAA Journal 21 (11) (1983) 1565–1570.

Appendix A. Derive $d\langle J \rangle/ds$

With a perturbation in s , the governing equation for u is:

$$\frac{d(u + \Delta u)}{dt} = f(u + \Delta u, s + \Delta s)$$

We define another quantity, η . As shown in fig A.11, assume that at time t , the difference of the new trajectory from the original one is $\Delta u^\perp(t)$. After Δt , neglecting higher order small quantities, this difference becomes $\Delta u^\perp(t) + (\partial_u f \Delta u^\perp(t) + \partial_s f \Delta s) \Delta t$. The projection of this new difference onto $V^0(t + \Delta t)$ is denoted by $-\eta f \Delta t \Delta s$; the projection onto V^\perp is $\Delta u^\perp(t + \Delta t)$.

Recall our definition of v and v^\perp , the equation for η is:

$$\frac{dv^\perp}{dt} = \partial_u f v^\perp + \partial_s f + \eta f \quad (\text{A.1})$$

Subtract equation A.1 from 3, we get:

$$\frac{d(v - v^\perp)}{dt} = \partial_u f(v - v^\perp) - \eta f$$

By our definition of ξ ,

$$\frac{d(\xi f)}{dt} = \partial_u f(\xi f) - \eta f$$

by Leibniz rule for differential,

$$\frac{d(\xi f)}{dt} = \xi \frac{df}{dt} + \frac{d\xi}{dt} f$$

Recall the chain rule for differential,

$$\partial_u f(\xi f) = \xi \partial_u f(f) = \xi (\partial_u f \frac{du}{dt}) = \xi \frac{df}{dt}$$

Finally, we find that η is indeed:

$$\eta = -\frac{d\xi}{dt} \quad (\text{A.2})$$

Above we looked at how to compare the new and base trajectories within the same amount of time Δt . But if we always compare the two trajectories at the same time frame, soon they will part from each other. This would make the higher order small quantities no longer negligible, hence our following analysis not working.

Alternatively, we vary Δt so that the states of the two trajectories remain close. In time Δt , the new trajectory moves a length of $f\Delta t - \eta f\Delta t\Delta s$. So the new speed is $(1 - \eta\Delta s)f$. Hence the new trajectory needs time $\Delta t/(1 - \eta\Delta s) \approx \Delta t(1 + \eta\Delta s)$ to cross the same length $f\Delta t$.

If we compare the point on base trajectory at time $(t + \Delta t)$ with the point on the perturbed trajectory at time $t + \Delta t(1 + \eta\Delta s)$, the distance is $\Delta u^\perp(t + \Delta t)$. Notice that $\Delta u^\perp(t) \approx v^\perp\Delta s$. If we have a bounded v^\perp , as claimed by the shadowing lemma [28], the corresponding Δu^\perp will always be in the same order of Δs . In other words, if we compare trajectories at different time frames, the points we are comparing can remain close to each other in the phase space.

The $J_{new}\Delta t_{new}$ on this small section of new trajectory is:

$$\begin{aligned} & J_{new}\Delta t_{new} \\ &= (J + \partial_u J \Delta u^\perp)(1 + \eta\Delta s)\Delta t \\ &= J\Delta t + \partial_u J \Delta u^\perp \Delta t + J\eta\Delta s\Delta t \end{aligned} \quad (\text{A.3})$$

Integrate above equation over time period $[0, T]$ and neglect higher order small quantities, the difference in averaged J is:

$$\begin{aligned} & \frac{1}{T_{new}} \int_0^{T_{new}} J_{new} dt - \frac{1}{T} \int_0^T J dt \\ &= \frac{1}{\int_0^T (1 + \eta\Delta s) dt} \int_0^T (J + \partial_u J \Delta u^\perp + J\eta\Delta s) dt - \frac{1}{T} \int_0^T J dt \\ &= \frac{\Delta s}{T} \int_0^T [\partial_u f v^\perp + \partial_s J + \eta(J - \langle J \rangle)] dt \end{aligned} \quad (\text{A.4})$$

Let $\Delta s \rightarrow 0$, we have the formula for $d\langle J \rangle_\infty/ds$:

$$\frac{d\langle J \rangle_\infty}{ds} \approx \frac{1}{T} \int_0^T [\partial_u f v^\perp + \partial_s J + \eta(J - \langle J \rangle_T)] dt \quad (\text{A.5})$$

The approximation is due to we are not integrating over an infinitely long trajectory. Apply equation A.2, we can see this is exactly the formula in equation 12.

From this deduction we can see why we want v^\perp to be small: our analysis requires neglecting higher order small quantities. If v^\perp grows exponentially, our analysis here is no long valid.

Appendix B. Finite difference NILSS method

We can use finite difference results to approximate all the tangent solutions used in NILSS method. In fact, we only need to approximate v^* and W . Once

their approximations are obtained, other parts of the algorithm follow.

To achieve this, first we compute a baseline primal solution u_b , which satisfies equation 1 with initial condition u_0 . Here u_0 is an arbitrary state on the attractor. Then we change s to $s + \Delta s$, and solve for u^* , which satisfies the perturbed governing equation with the same initial condition u_0 . Now we have approximation for v^* :

$$v^* \approx \frac{u^* - u_b}{\Delta s}$$

We solve for u^w by keeping same s but use initial conditions $u_0 + \Delta u_0$, where Δu_0 is random perturbation. The approximation for a homogeneous tangent solution w is:

$$w \approx u^w - u_b$$

The benefit of this finite difference version of NILSS is that it is truly non-intrusive. In fact, it even no longer requires a tangent solver, all it needs is a simulation software which can solve for the primal solution.

The downside is that, the approximation by finite difference may incur additional error. Also, when deciding the time segment length ΔT , there is an extra requirement, that is, the perturbation do not grow too large. Otherwise, the perturbation may fall out of the linear region, and the finite difference no longer approximates the tangent solution.

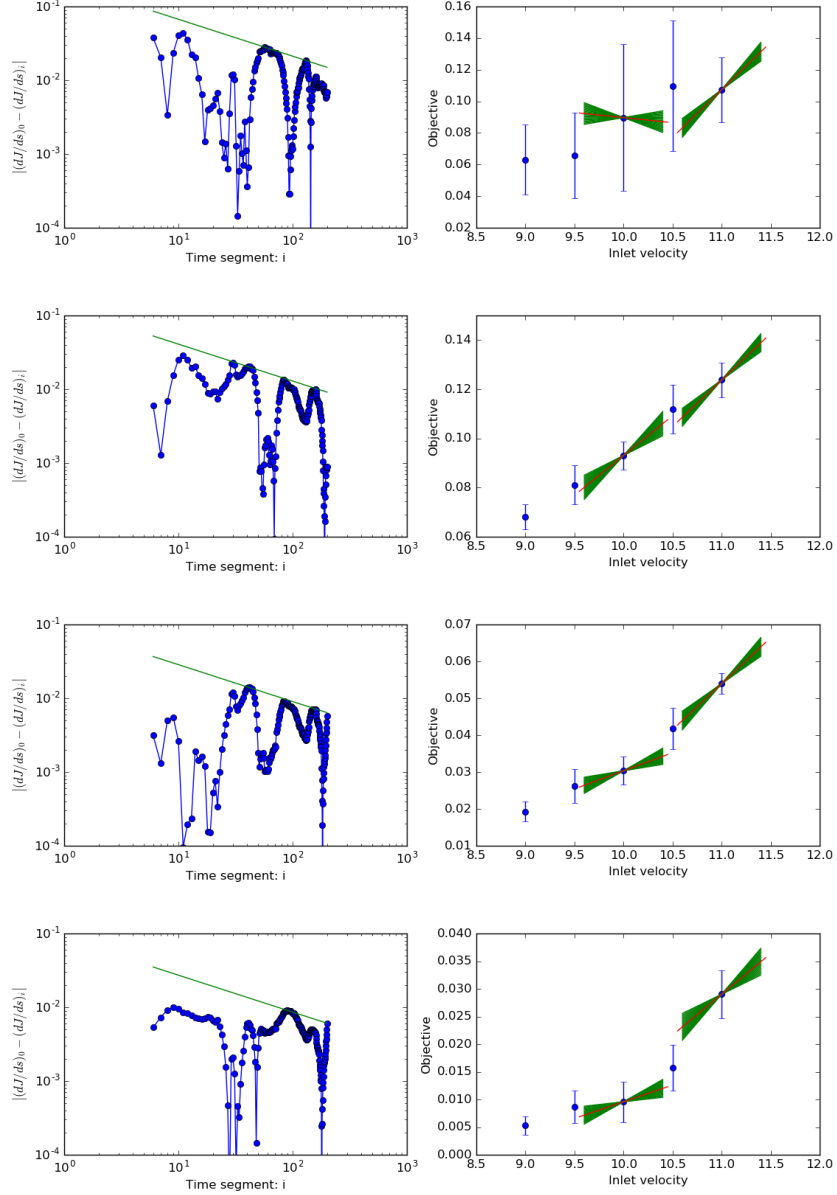


Figure 10: Sensitivity computed by NILSS. From top to bottom the objective function is the long-time average of U_x/U_{x0} , $(U_x/U_{x0})^2$, $(U_x/U_{x0})^4$, and $(U_x/U_{x0})^8$. Left column: sensitivity computed by increasing number of segments, the lines indicates confidence intervals for sensitivities. Right column: sensitivity plotted with objectives for adjacent parameters, the bars and wedges indicate confidence intervals of the objectives and sensitivities, respectively.

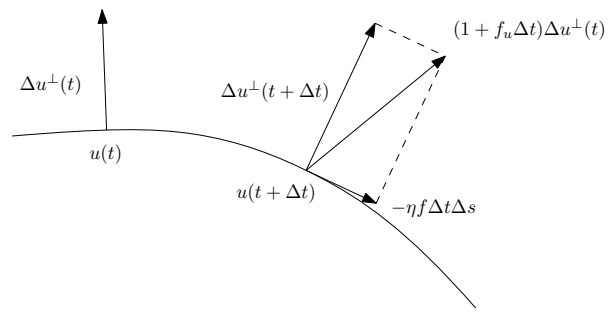


Figure A.11: Perturbation on the trajectory due to perturbation on the parameter